Available online at www.sciencedirect.com

ScienceDirect

Geochimica et Cosmochimica Acta 215 (2017) 105–121

Geochimica et Cosmochimica Acta

www.elsevier.com/locate/gca

On the hydration of olivine in ultramafic rocks: Implications from Fe isotopes in serpentinites

Sean R. Scott [a,b,*], Kenneth W.W. Sims [a,b], Bryce R. Frost [b], Peter B. Kelemen [c], Katy A. Evans [d], Susan M. Swapp [b]

[a] *Wyoming High Precision Isotope Laboratory, Department of Geology and Geophysics, University of Wyoming, Laramie, WY 82072, United States*

[b] *Department of Geology and Geophysics, University of Wyoming, Laramie, WY 82072, United States*

[c] *Lamont-Doherty Earth Observatory, Columbia University, Palisades, NY 10964, United States*

[d] *Department of Applied Geology, Curtin University, GPO Box 1987, WA 6845, Australia*

Received 18 August 2016; accepted in revised form 7 July 2017; available online 15 July 2017

Abstract

The behavior of Fe during serpentinization largely controls the potential for oxidation-reduction reactions and energy budget for serpentinite-hosted microbial communities. We present Fe isotope data for mineral separates from a partially serpentinized dunite from New Caledonia to understand the behavior of Fe during serpentinization processes. Our new Fe isotope data in mineral separates is compared to existing data from whole rock studies of serpentinites, which have generally concluded that Fe mobility during serpentinization is restricted to the highest temperatures of serpentinization in subduction zones. Measurements of mineral separates from New Caledonia show significant Fe isotope fractionations, with serpentine-brucite mixtures having the lowest $\delta^{56}Fe \sim -0.35‰$ and magnetite having the highest $\delta^{56}Fe \sim +0.75‰$. Olivine, orthopyroxene, and the whole rock composition are all within error of $\delta^{56}Fe = 0.00‰$. Fe isotope thermometry between mineral phases reveals two distinct temperatures of equilibration, one for the mantle olivine and pyroxene (~1325 °C), and a second, much lower temperature (~335 °C) for the serpentinite assemblage. The combined isotopic, mineralogical and geochemical data indicate that during the magnetite-forming stage of serpentinization, a pore fluid in equilibrium with the mineralogical assemblage evolves to higher Fe concentrations as serpentinization proceeds. When this pore fluid is removed from the serpentinizing environment, the total abundance of Fe removed from the rock in the pore fluid is much less than the bulk rock Fe and has a minimal effect on the overall rock composition.

Published by Elsevier Ltd.

Keywords: Serpentinization; Fe isotopes; New Caledonia

1. INTRODUCTION

Serpentinization, initiated by reactions between olivine and water, occurs across a spectrum of tectonic settings, from deep-ocean hydrothermal systems to subduction zones to subaerial continental hydrothermal systems. During serpentinization, ultramafic minerals such as olivine, are hydrated and form new mineral assemblages, causing large volume expansion and heat production due to exothermic reactions. In near surface environments, serpentinization can occur at temperatures from ~20 °C to greater than 400 °C (e.g., Barnes et al., 1978; Allen and Seyfried, 2004), and the thermodynamic stability of antigorite (up to ~640 °C, Bromiley and Pawley, 2003) suggests that serpentinization reactions also occur deeper within the Earth (e.g., subduction zones).

* Corresponding author at: Department of Geology and Geophysics, University of Wyoming, Laramie, WY 82072, United States.

E-mail address: sscott25@uwyo.edu (S.R. Scott).

http://dx.doi.org/10.1016/j.gca.2017.07.011

0016-7037/Published by Elsevier Ltd.

Where olivine and water (either meteoric water, seawater, or deep crustal or subduction zone fluids) interact, new mineral assemblages provide a record of these fluid-rock interactions. In the oceanic crust, intrusive igneous rocks, many of which contain high modal olivine, provide an abundance of evidence for deep seawater circulation and hydration of olivine (e.g., Bach et al., 2006; Beard et al., 2009); thus hydration of olivine is considered a relatively ubiquitous process throughout the oceanic lithosphere (Iyer et al., 2010). Hydrated oceanic crust eventually proceeds into subduction zones, where prograde metamorphic water-rock reactions involve progressive increases in temperature and pressure as the subducting slab carries mafic and ultramafic rocks into the mantle. The highest temperatures of serpentinization occur in this setting and produce antigorite serpentine assemblages (antigorite is the more stable serpentine polymorph at high temperatures; Hilairet et al., 2006). Serpentinization reactions result in dehydration of the subducting slab, fluid flux into the overlying mantle, and/or partial melting of both the subducting slab and overlying mantle depending on the tectonic arrangement of the subduction zone (e.g., Yogodzinski et al., 2015). Importantly, as fluids are desorbed from the subducting slab via dehydration reactions, serpentinization likely occurs in the overlying mantle wedge (Hyndman and Peacock, 2003). When these geologic systems are obducted onto the continents as ophiolites, low temperature serpentinization occurs near the surface due to chemical weathering by meteoric water (e.g., Oman, New Caledonia; Barnes et al., 1978; Streit et al., 2012). As such, serpentinization is the fundamental mechanism responsible for fluid migration in geologic settings where olivine is present, and thus plays a critical role in arc volcanism, geochemical cycling between the oceanic lithosphere and the hydrosphere, seafloor ecosystems, and continental hydrothermal systems.

At all temperatures of serpentinization, Fe plays a key role in serpentinite mineral assemblages. Fe is a major component of ultramafic rocks and found ubiquitously in the serpentinite mineral assemblages in multiple oxidation states. Fe is likely to be mobilized during dehydration processes in subduction zones (Debret et al., 2016), and while high concentrations of Fe have been observed in some seafloor ultramafic vent fluids (e.g., Schmidt et al., 2007), direct evidence for Fe mobility during seafloor serpentinization is not clear in abyssal serpentinites (e.g., Craddock et al., 2013), and low temperature vent fluids typically contain very little Fe (Barnes et al., 1978; Marques et al., 2008; Chavagnac et al., 2013). However, the presence of magnetite in serpentine veins requires that Fe is mobile at least on the size scale (~0.1–10 mm) of the mineral grains (e.g. Frost et al., 2013). Fe isotopes have provided insights into Fe cycling during hydrothermal alteration of mafic rocks (e.g., Rouxel et al., 2003, 2008). Ultramafic rocks, which have high modal abundance of olivine, provide important insights into the roots of a hydrothermal system, and as of yet, there have been no studies of inter mineral Fe isotope variations in serpentinites.

Here we present Fe isotope measurements in mineral separates from a partially serpentinized dunite from New Caledonia to evaluate the relationships between fluids and minerals during fluid-rock interaction in the ultramafic oceanic crust. As we will show, these data enable us to address specific aspects of serpentinization: (1) the scale of Fe mobility during serpentinization; (2) the temperature of serpentinization based on theoretical fractionation models; and, (3) the water/rock ratio and possible pore fluid evolution during and after the serpentinization process occurs.

2. BACKGROUND

2.1. The process of serpentinization

Serpentinization has been studied in a wide range of settings using a variety of techniques. Detailed textural and geochemical data has been extracted from ultramafic rocks preserved in ophiolites (e.g., Coleman and Keith, 1971; Evans, 1977; Toft et al., 1990; Boudier et al., 2010; Barnes et al., 2013; Frost et al., 2013) and rocks recovered from drilling and dredging of the oceanic crust (e.g., Bach et al., 2006; Frost et al., 2008; Beard et al., 2009; Andreani et al., 2013; Rouméjon and Cannat, 2014). These studies have revealed the complicated nature of the serpentinization process, specifically: the textural variations associated with different stages of serpentinization (e.g., mesh texture vs. large through going serpentine veins); nanoscale interlayering of brucite and serpentine detected by TEM (Bach et al., 2006); and, the variable oxidation state of Fe in the most abundant mineral phases (e.g., serpentine, magnetite, and brucite).

In addition to textural data on rock samples, exploration and sampling of hydrothermal vent systems on the seafloor have provided fundamental insights into their geology and fluid-rock interaction processes in the oceanic lithosphere (e.g., Delaney et al., 1992; Von Damm et al., 1997; Von Damm, 2000; Kelley et al., 2001; Charlou et al., 2002). Seafloor hydrothermal systems hosted by ultramafic rocks often contain high concentrations of Fe in vent fluids (Charlou et al., 2002; Schmidt et al., 2007). Thermodynamic modeling of serpentinization has also placed constraints on the relative timing and formation of serpentinite assemblages, as well as the potential for serpentinite hydrothermal systems to support chemotrophic life (e.g., Klein and Bach, 2009; Evans et al., 2013; Klein et al., 2014; Seyfried et al., 2015). Additionally, lab experiments involving seawater and ultramafic rocks have provided a time-integrated perspective on changes in mineralogy and associated hydrothermal fluid during serpentinization, showing that reactions between seawater and ultramafic rocks are generally accompanied by increases in Fe concentrations in the reacting fluids (e.g., Seyfried and Dibble, 1980; Janecky and Seyfried, 1986; Allen and Seyfried, 2004; Seyfried et al., 2007). Nonetheless, the processes occurring during the earliest stages of serpentinization are still debated (Frost and Beard, 2007; Evans, 2008; Beard et al., 2009; Evans, 2010; Katayama et al., 2010; Frost et al., 2013; Miyoshi et al., 2014). Specifically, the conditions for magnetite formation and the relationships between iron oxidation-reduction processes and

mineral assemblages are controversial (McCollom et al., 2016). Furthermore, while serpentinization occurs in an open system, the timing and nature of this open system behavior remains ambiguous and poorly characterized.

In the past ~15 years, researchers have begun to evaluate the importance of Fe in hydrothermal systems; of particular interest has been the application of stable Fe isotopes to evaluate connections between hydrothermal vent fluids and oceanic crust alteration. Despite considerable work, the mobility of Fe during seafloor serpentinization remains uncertain. Early research demonstrated the fractionation of Fe isotopes in seafloor hydrothermal systems, and suggested that this may be the cause of Fe isotopic variability observed in Fe-Mn crusts (Sharma et al., 2001). However, Severmann et al. (2004) showed that the isotopic compositions of vent fluids at the Rainbow vent site on the Mid-Atlantic ridge have not changed over the last ~16,000 years, suggesting that Fe isotopic variations in Fe-Mn deposits and by inference ocean waters are not a function of variations in hydrothermal input, but rather variations in terrestrial and/or atmospheric (aerosol) input (Zhu et al., 2000; Beard et al., 2003).

The Fe isotopic compositions of oceanic hydrothermal vent fluids are uniformly low relative to chondritic compositions (Rouxel et al., 2008), and reveal a small fractionation ($\delta^{56}Fe \sim 0.3‰$) between the bulk mafic oceanic crust and the Fe being removed in hydrothermal fluids. Mafic crust becomes progressively more isotopically heavy with increasing degree of alteration, which is balanced by isotopically light Fe in hydrothermal fluids (Rouxel et al., 2003). This Fe isotope fractionation is seen not only in the bulk mafic crust, but even more so in the alteration mineral assemblages which show even larger ranges of Fe isotope fraction (Rouxel et al., 2003). Thus, seafloor hydrothermal systems are relatively well understood from an Fe cycling perspective in locations where mafic rocks are being altered (Rouxel et al., 2003, 2008), while hydrothermal systems involving ultramafic rocks are poorly understood from an inter mineral perspective.

Discoveries of large exposures of ultramafic rocks along active tectonic margins on the seafloor, especially along slow and ultra-slow spreading ridges (e.g., Cannat et al., 1995; Carlson, 2001; Smith et al., 2006), suggest that these ultramafic systems likely play an important role in geochemical exchange between the hydrosphere and lithosphere where ultramafic rocks are exposed. Severmann et al. (2004) showed that fluids emanating from ultramafic hydrothermal systems contain isotopically light Fe, suggesting that, like mafic systems, isotopically light Fe is removed from the bulk rocks in the subsurface, leaving behind a relatively isotopically heavy residue. However, more recent studies of Fe isotopic compositions on whole rocks from ultramafic settings (abbysal serpentinites-Craddock et al., 2013; Purang ophiolite-Su et al., 2015; alpine serpentinites-Debret et al., 2016) show different results. In abyssal peridotites, Craddock et al. (2013) demonstrated a relatively uniform and nearly chondritic Fe isotopic composition despite large variations in the degree of alteration (i.e., serpentinization). Whereas, Debret et al. (2016) noted a slight increase in the Fe isotopic composition of Alpine serpentinites in the higher temperature assemblages (i.e., those bearing antigorite), and attributed this isotopic shift to Fe mobility during dehydration of the subducting slab. While actively serpentinizing systems are difficult to sample on the seafloor, studies of Fe isotopes in well-studied ophiolites and abyssal ultramafic rocks can provide insight into the significance of ultramafic hydration and the geochemical cycling associated with hydrothermal alteration of the ultramafic lithosphere. In turn, measurements of mineral separates in these serpentinizing systems provide insight into the mass balance relationships associated with Fe mobility in hydrothermal ultramafic systems.

2.2. Petrology of New Caledonia ophiolite

The partially serpentinized dunite chosen for this study (NC09-5) is from New Caledonia, and has been studied in detail by Evans et al. (2013), Frost et al. (2013) and Mothersole et al. (in press). The island of New Caledonia contains an ophiolite sequence that was emplaced sometime prior to 27 Ma, which is the age of subduction related plutons intruding the sequence (Cluzel et al., 2006). Eclogite gneisses representing peak metamorphic conditions in New Caledonia record temperatures up to ~600 °C. However, tectonic models for the emplacement of the New Caledonia ophiolite sequence indicate that this ophiolite did not experience significant burial driven changes in pressure and/or temperature (Aitchison et al., 1995). New Caledonia ophiolitic exposures are dominated by partially serpentinized harzburgite and dunite with minor gabbro. Natural seepages of relatively low temperature (~26–40 °C), high pH (~11) fluids have been discovered within the ophiolite sequence (Barnes et al., 1978; Deville and Prinzhofer, 2016), and these fluids could provide a mechanism for modern serpentinization processes occurring at depth (Barnes et al., 1978). However, as will be discussed below, the presence of magnetite in our rocks demonstrate that the dominant imprint of serpentinization on NC09-5 occurred at higher temperatures.

Three distinct types of serpentine veins have been identified in New Caledonia, all of which were determined to be dominantly lizardite serpentine by Raman spectroscopy (Frost et al., 2013). The earliest veins (type 1) do not extend across more than a single olivine grain and contain only serpentine and brucite. Type 2 veins typically cut across multiple olivine grains and also cross cut type 1 veins. Type 2 veins contain magnetite cores and less brucite than type 1 veins (Fig. 1). Type 3 veins are the largest, contain abundant magnetite and the most Mg-rich serpentine, and cross cut both type 1 and type 2 veins. While all three types of veins likely form simultaneously during the serpentinization process, the type 1 veins are the first to form in the initial stages of fluid infiltration (i.e., type 2 and type 3 veins do not form without the prior formation of type 1 veins). The sample chosen for this study contains only type 1 and type 2 veins because these veins represent the earliest stages of serpentinization, and our goal was to evaluate the early stages without the influence of large scale open system processes that may occur in other serpentinization settings (e.g., subduction zones, Debret et al., 2016).

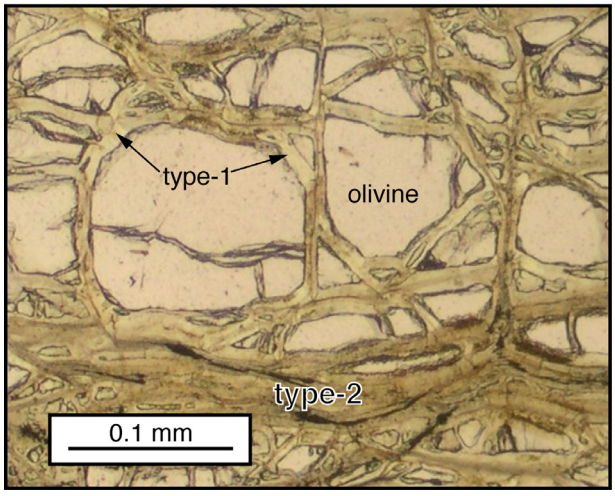

Fig. 1. Photomicrograph of NC09-05 showing the textural relationships between olivine, type 1, and type 2 serpentine veins (after Frost et al., 2013). The mass balance relationships in Eqs. (1) and (2) are represented petrographically in this image. Water is added to olivine to form the type 1 veins, composed of only serpentine and brucite. These veins are later further altered to form the serpentine and magnetite assemblage. In this image, magnetite in type 2 veins is never in contact with olivine, suggesting this mineral does not form directly from olivine. The textural relationships in NC09-5 have been observed elsewhere (Bach et al., 2006; Beard et al., 2009; Katayama et al., 2010; Miyoshi et al., 2014).

Detailed electron probe analyses of the constituent minerals from NC09-5 revealed relatively homogeneous olivine ($X_{Mg} = 0.911 \pm 0.001$) and pyroxene ($X_{Mg} = 0.916 \pm 0.002$) compositions, while serpentine and brucite compositions were more variable. Brucite in type 1 serpentine veins was more Fe-rich than brucite in type 2 veins ($X_{Mg} = 0.819$ vs. 0.836), as well as the serpentine ($X_{Mg} = 0.923$ vs. 0.932). However, as the magnetite bearing veins become larger, serpentine compositions tend to deviate to Mg-rich and Fe-rich varieties, with $X_{Mg} = 0.941$ and 0.909, respectively (Frost et al., 2013).

Progressive multi-stage serpentinization reactions explain the formation of type 1, type 2, and type 3 veins. The reactions to form magnetite in the New Caledonia system occur in two stages:

$$\underset{olivine}{2(Mg,Fe)_2SiO_4} + \underset{water}{3H_2O} \rightarrow \underset{serpentine}{(Mg,Fe)_3Si_2O_5(OH)_4} + \underset{brucite}{(Mg,Fe)(OH)_2} \quad (1)$$

$$\underset{Fe\,in\,brucite}{15Fe(OH)_2} + \underset{aqueous\,silica}{4SiO_2} \rightarrow \underset{Fe\,in\,serpentine}{2Fe_3Si_2O_5(OH)_4} + \underset{magnetine}{3Fe_3O_4} + \underset{water}{8H_2O} + \underset{hydrogen}{3H_2} \quad (2)$$

Reaction (2) occurs in the presence of native Fe metals, which can form from Fe in solution by the following reaction (after Frost, 1985):

$$\underset{Fe\,in\,solution}{Fe^{2+}} + \underset{hydrogen}{H_2} \rightarrow \underset{Fe\,metal}{Fe^0} + \underset{protons}{2H^+} \quad (3)$$

Reactions (1) and (2) are written to illustrate the hypothesis that magnetite does not form directly from olivine, as has been proposed to occur in other locations based on detailed textural and geochemical studies (e.g. Bach et al., 2006; Beard et al., 2009; Katayama et al., 2010; Miyoshi et al., 2014). Although the source of aqueous silica in reaction (2) is equivocal (Beard et al., 2009), Miyoshi et al. (2014) have shown that the external source of silica required for magnetite formation might be derived from hydration of orthopyroxene:

$$\underset{orthopyroxene}{3(Mg,Fe)SiO_3} + \underset{water}{3H_2O} \rightarrow \underset{serpentine}{(Mg,Fe)_3Si_2O_5(OH)_4} + \underset{aqueous\,silica}{SiO_2} \quad (4)$$

Frost et al. (2013) noted the presence of serpentinized orthopyroxene in the NC09-5 sample, lending credence to the two-stage magnetite formation hypothesis in New Caledonia. Fe isotope data in mineral separates will provide additional quantitative analysis of the reactions taking place during serpentinization.

3. METHODS

3.1. Mineral separation and Fe isotope analysis

The sample was disaggregated using an electron pulse disaggregator to prevent Fe contamination from jaw crushing and to crush the rock to smaller pieces for further processing. The resulting disaggregated sample was sieved, and the smallest size fractions were subjected to a Frantz magnetic separator to divide magnetic minerals (i.e., magnetite and awaruite) from non-magnetic minerals (e.g., olivine, serpentine). Magnetic and non-magnetic fractions were rinsed in deionized water. Individual mineral phases were then handpicked under a microscope. Type 2 serpentine veins were easily identified in thin section because they typically cut across multiple olivine grains and contain magnetite. In the mineral separates, type 2 veins are identified by their relatively large grain size, fibrous crystal habit, and the presence of magnetite in vein cores, thus we are confident in our identification of this critical phase.

Grain sizes generally ranged from 0.1 mg to ~5 mg, and total Fe abundances for each grain was >20 μg. Individual silicate minerals were dissolved in individual Teflon beakers using a combination of ultra-pure HNO_3-HCl-HF. Awaruite grains were dissolved using ultra-pure Aqua Regia. Magnetite grains were dissolved in 23 ml Teflon Parr bombs using ultra-pure Aqua Regia. Once fully digested, samples were dried and redissolved in concentrated HNO_3 to ensure complete oxidation of Fe for purification using anion exchange resin. This concentrated HNO_3 solution was dried, and samples were redissolved in 0.5 ml 6 N HCl + 0.002% H_2O_2 for purification. Samples were loaded onto 0.5 ml of AG1-X8 100–200 mesh anion exchange resin and 6 ml of 6 N HCl + 0.002% H_2O_2 was used to elute interfering matrix elements. Fe was subsequently collected using 4 ml 0.05 N HCl following similar procedures as described by Craddock and Dauphas (2010) and Millet et al. (2012). Rock standards were used to assess and ensure quantitative yields from anion exchange columns.

Chemically separated and purified Fe aliquots were dried and then redissolved in 1 N (5%) HNO_3 at least 2 h prior to analysis. These Fe aliquots were diluted to match standard Fe concentrations, generally ~400 ppb. The Fe

isotopes were analyzed on a ThermoFinnigan NeptunePlus MC-ICPMS at the University of Wyoming High-Precision Isotope Laboratory using medium-resolution mode and an Apex desolvating nebulizer introduction system. Sample-standard bracketing was used to correct for mass bias. Each individual sample was analyzed at least three times, and up to ten times, between individual IRMM-014 standard analyses. Reported errors are the 2 standard deviation confidence intervals for each individual grain average of these analyses. Additional standards (BCR-2, BHVO-2, RGM-2, TML, and an internal FeSpec ICP solution) were measured to assess the long-term reproducibility of measurements (see Section 4.2 for a discussion of Data Quality Assurance).

3.2. Geochemical modeling

Geochemical modeling of reactions between mafic minerals and seawater was carried out using Geochemist's Workbench® (GWB) version 9.0 (Bethke and Yeakel, 2012) Modeling used equilibrium titration mode initially, followed by flow through mode for certain reactions to assess two perspectives of the same conceptual model. In the titration model, reactants (in this case olivine or pyroxene) are added to the initial system (seawater), and the fluid and minerals remain in equilibrium throughout the model. In flow through models, precipitated minerals do not maintain equilibrium with the liquid, and are unable to redissolve or form new minerals. Seawater composition was obtained from Brown et al. (1989), and reactions with orthopyroxene and olivine were modeled. Olivine and pyroxene were treated as mechanical mixtures of forsterite/fayalite and ferrosilite/enstatite, respectively. Reactions were modeled at 300 °C using only olivine or pyroxene to determine relative effects of each mineral type on fluid chemistry. Water/rock sensitivity was modeled to assess variations in mineral phases dependent on water/rock ratios. Results were compared to high temperature hydrothermal experiments (Seyfried and Dibble, 1980; Janecky and Seyfried, 1986) and vent fluid compositions (Charlou et al., 2002; Schmidt et al., 2007) to assess the validity of the models.

4. RESULTS

4.1. Fe isotope variation in New Caledonia sample NC09-5

Iron isotopic compositions for mineral separates from NC09-5 and the whole rock are presented in Table 1 and Fig. 2. All samples were measured by sample-standard bracketing and are expressed in delta notation relative to IRMM-014. A significant range ($\delta^{56}Fe \sim 1.1‰$) of Fe isotope ratios was measured in various mineral phases, with all samples lying along a triple isotope mass-dependent fractionation line (Fig. 2). Type 2 veins (a mixture of brucite and serpentine; Frost et al., 2013) have the lowest values with $\delta^{56}Fe$ ranging from −0.31 to −0.36‰. Magnetite has the highest value at $\delta^{56}Fe = +0.77‰$, and awaruite also has relatively high values from +0.28 to +0.39‰. Olivine $\delta^{56}Fe$ values range from −0.04 to +0.05‰, and pyroxene $\delta^{56}Fe$ values range from −0.01 to +0.06‰. The whole rock has $\delta^{56}Fe = -0.02‰$. Fe isotopic compositions for each mineral separate group are within analytical reproducibility, i.e., there is no discernable difference in isotopic composition within each mineral type. In addition, the isotopic compositions of olivines, orthopyroxenes, and the whole

Table 1
Iron isotopic compositions of mineral separates and the whole rock.

Sample	Type	$\delta^{56}Fe$[a]	2stderr	$\delta^{57}Fe$[a]	2stderr	n
NC09-5 A1	Awaruite	0.276	0.061	0.379	0.072	9
NC09-5 A2	Awaruite	0.317	0.049	0.482	0.057	6
NC09-5 A3	Awaruite	0.387	0.064	0.543	0.041	3
NC09-5 M14	Magnetite	0.770	0.042	1.140	0.050	3
NC09-5 O2	Olivine	−0.017	0.085	−0.047	0.156	3
NC09-5 O3	Olivine	−0.035	0.051	0.025	0.100	6
NC09-5 O4	Olivine	0.047	0.024	0.107	0.082	3
NC09-5 O5	Olivine	0.030	0.136	0.083	0.195	3
NC09-5 P0	Orthopyroxene	0.017	0.147	0.030	0.090	3
NC09-5 P1	Orthopyroxene	0.000	0.064	−0.027	0.079	3
NC09-5 P2	Orthopyroxene	−0.007	0.027	0.000	0.114	3
NC09-5 P3	Orthopyroxene	0.013	0.048	0.007	0.024	3
NC09-5 P4	Orthopyroxene	0.030	0.064	0.050	0.090	3
NC09-5 P5	Orthopyroxene	0.063	0.064	0.040	0.090	3
NC09-5 S5	Type-2 vein	−0.357	0.070	−0.561	0.110	10
NC09-5 S6	Type-2 vein	−0.320	0.093	−0.595	0.100	8
NC09-5 S7	Type-2 vein	−0.347	0.071	−0.463	0.116	3
NC09-5 S8	Type-2 vein	−0.307	0.035	−0.440	0.046	3
NC09-5 WR	Whole rock	−0.024	0.024	−0.029	0.087	3

[a] δ values relative to IRMM-014.

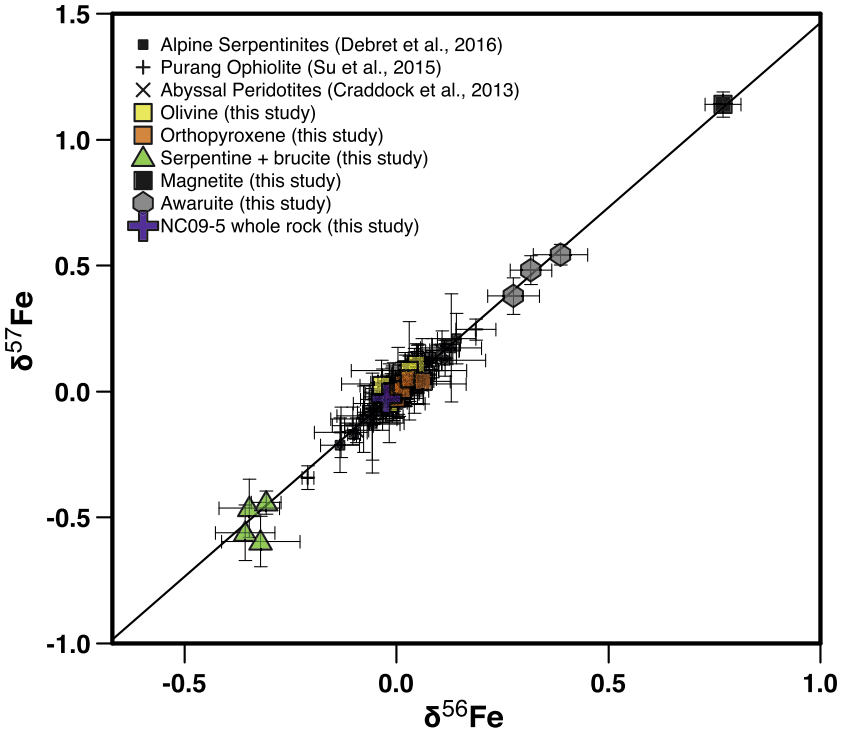

Fig. 2. Fe isotopic compositions (δ^{57}Fe vs. δ^{56}Fe) of mineral separates plotted along a mass-dependent fractionation line compared to whole rock literature data (Craddock et al., 2013; Su et al., 2015; Debret et al., 2016) for abyssal serpentinites and ophiolite serpentinites. Combinations of brucite and serpentine (serpentine + brucite) represent type 2 veins, with brucite and serpentine interlayered at nanometer scales.

rock span a relatively small range of values centered on δ^{56}Fe ~ 0.00‰.

4.2. Data Quality Assurance

Replicate analyses of BCR-2 ($n = 65$) gave an average value of 0.107 ± 0.021‰ δ^{56}Fe and 0.146 ± 0.028‰ δ^{57}Fe which is within error of recently reported values (Fig. 3). Results for standard analyses and reference values for BCR-2, BHVO-2, and RGM-2 are provided in Table 2. The long-term reproducibility of BCR-2 at one standard deviation was 0.084 and 0.114 for δ^{56}Fe and δ^{57}Fe, respectively. This reproducibility is comparable to the estimate for external precision using sample-standard bracketing of ca. 0.10‰ and ca. 0.15‰ for δ^{56}Fe and δ^{57}Fe (2 SD; Weyer and Schwieters, 2003).

4.3. Geochemical modeling results

Mineral phases precipitated in Geochemist Work Bench® (GWB) reaction models are broadly consistent with observed serpentinite assemblages (Fig. 4). In the olivine-seawater reaction, antigorite was the dominant serpentine phase, along with brucite, hematite and magnetite. Antigorite and brucite were initially present in the seawater-pyroxene titration reaction but were subsequently replaced by talc. Minor amounts of pyrite and anhydrite were present in both reactions. No other serpentine minerals were saturated during these reactions. Flow through and titration models produced the same mineral assemblages; however, rather than certain minerals dissolving (observed in titration models), precipitated minerals remained throughout flow through reaction models (e.g. hematite; Fig. 5). When antigorite was suppressed, chrysotile became the serpentine mineral. The chemical compositions of chrysotile and antigorite are essentially identical; thus, suppressing antigorite and precipitating chrysotile did not affect the chemistry of the fluid. The thermodynamic database in GWB used for the models does not contain data for lizardite, however recent thermodynamic data for serpentine minerals shows similar results for chrysotile and lizardite (Holland and Powell, 2011).

The water/rock ratio of the system played a significant role in the relative proportions of Fe-oxides that precipitate throughout the reactions. In general, high water/rock ratios produce more hematite, while low water/rock ratios produce more magnetite (Fig. 6). Differences between titration models and flow through models in olivine-seawater reactions are most apparent in the Fe-oxides while the proportions of serpentine and brucite remain essentially the same for either type of reaction. At low water/rock ratios in titration models, hematite does not precipitate at all, while at high water rock/ratios, magnetite does not precipitate (Fig. 6). In contrast, magnetite and hematite are both present at most water/rock ratios in flow through models with the exception of the most extreme water/rock ratio values (Fig. 6).

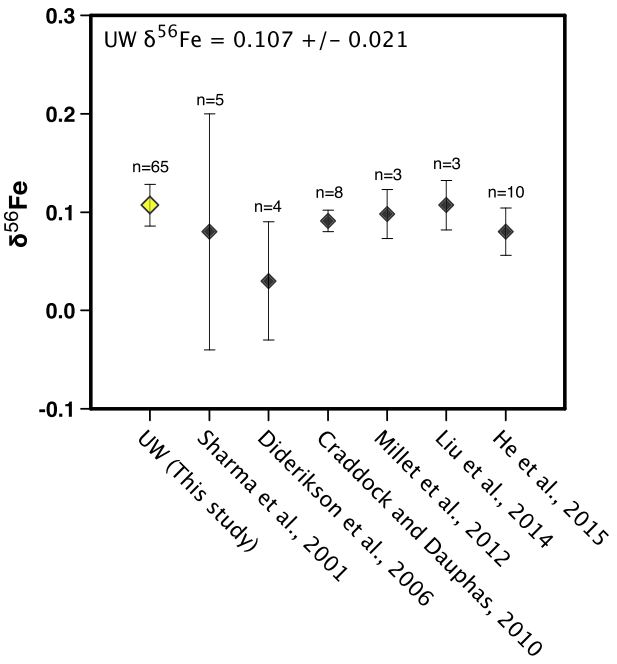

Fig. 3. Fe isotopic compositions of BCR-2 from University of Wyoming (UW) compared to published values (Sharma et al., 2001; Dideriksen et al., 2006; Craddock and Dauphas, 2010; Millet et al., 2012; Liu et al., 2014; He et al., 2015).

5. DISCUSSION

5.1. Implications for mass transfer during serpentinization

One of the most interesting results of our study is the relatively minor impact of serpentinization on the bulk Fe in the rock despite large inter-mineral isotopic fractionations. Frost et al. (2013) report relatively large variations in the internal composition of individual serpentine veins, with average compositions of type-2 serpentine veins ranging from 4.54 to 6.56 wt.% FeO. Calculated mixing relationships between magnetite and type 2 veins suggest that ~3% magnetite and 97% type 2 vein with ~6.18 wt.% FeO approximates the isotopic composition of the olivine (Fig. 7), consistent with the relatively minor amounts of magnetite observed in the serpentine veins compared to serpentine and brucite. The estimated serpentine FeO proportion is within the range of compositions observed by Frost et al. (2013), and likely represents a mixture between brucite and serpentine. The bulk rock has lower FeO than the olivine, which can be attributed to the effects of the lower FeO content of the orthopyroxene. The mass balance between the serpentinization assemblage and the olivine composition, both in Fe concentration and isotopic composition, suggests that very little Fe was added to or lost from the rock during the serpentinization process. In turn, this suggests that the hydration of ultramafic rocks (at least the early stages) in general does not have a large effect on the geochemical cycling of Fe in Earth's near surface systems. This lack of significant removal of Fe is in contrast to the dehydration processes associated with serpentinization in subduction zones, where Debret et al. (2016) have shown isotopic evidence for Fe mobility (discussed in more detail in Section 5.3).

5.2. Crystal chemical constraints on inter-mineral Fe isotope fractionation during serpentinization of peridotite

Our new data on mineral separates show that large Fe isotope fractionations occur during serpentinization. This observation is broadly consistent with the relative sense of fractionation described by the Mössbauer model (Polyakov, 1997; Polyakov and Mineev, 2000; Polyakov

Table 2
Fe isotopic compositions of standards measured at UW compared to literature values.

	Reference	$\delta^{56}Fe$[a]	±[c]	$\delta^{57}Fe$[a]	±[c]	n
BCR-2	Craddock and Dauphas (2010)	0.091	0.011	0.126	0.017	8
	Dideriksen et al. (2006)	0.030	0.060			4
	He et al. (2015)	0.080	0.024	0.123	0.036	10
	Liu et al. (2014)	0.107	0.025	0.170	0.013	3
	Millet et al. (2012)	0.098	0.025			3
	Sharma et al. (2001)	0.080	0.120	0.140	0.210	5
	UW[b]	0.107	0.021	0.146	0.028	65
BHVO-2	Craddock and Dauphas (2010)	0.114	0.011	0.174	0.016	12
	Dideriksen et al. (2006)	−0.030	0.070			2
	He et al. (2015)	0.112	0.021	0.163	0.040	27
	Liu et al. (2014)	0.121	0.049	0.175	0.064	12
	Millet et al. (2012)	0.128	0.019			
	UW[b]	0.120	0.019	0.204	0.035	21
RGM-2	Craddock and Dauphas (2010)	0.216	0.014	0.329	0.020	6
	UW[b]	0.179	0.015	0.322	0.023	3
FeSpec	UW[b] ICP standard	−0.466	0.021	−0.684	0.035	69

[a] δ values relative to IRMM-014.
[b] UW value as of January 5, 2016.
[c] UW errors are 2 standard error.

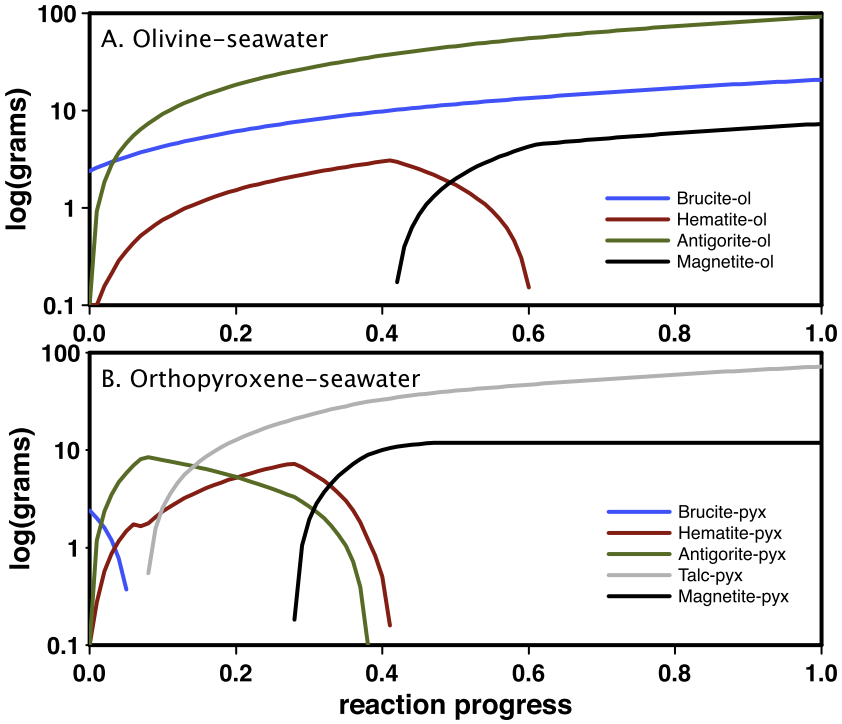

Fig. 4. Mineral assemblages precipitated during titration model reactions between seawater and olivine (a) and orthopyroxene (b). Minor amounts (<0.1 g) of anhydrite and pyrite are not shown. Mineral assemblages between olivine and orthopyroxene reactions are similar, with the exception that talc essentially replaces serpentine in the orthopyroxene reaction. Hematite is present in the initial stages of both reactions, but is eventually replaced by magnetite. The final assemblage of the olivine-seawater reaction (serpentine + brucite + magnetite) is consistent with the observed assemblage in NC09-5, with the caveat that the thermodynamic model predicts precipitation of antigorite (rather than lizardite or chrysotile). Regardless of the type of serpentine precipitated, the fluid in the model becomes enriched in Fe relative to the initial fluid composition (seawater).

et al., 2007), which predicts that magnetite should have the highest δ^{56}Fe and δ^{57}Fe of any of the minerals involved in this study. In addition, the Mössbauer model calculations indicate that native Fe metals should have lower δ^{56}Fe and δ^{57}Fe than magnetite, but higher than olivine or orthopyroxene, consistent with our observations. Mössbauer model fractionation factors are not available for serpentine group minerals, however Mössbauer data for sheet silicates with compositions most comparable to serpentine (chloritoids, Polyakov and Mineev, 2000) suggests these minerals will have lower δ^{56}Fe and δ^{57}Fe than olivine. The Fe isotopic compositions of serpentine are consistent with a similar type of behavior for serpentine group minerals and chloritoids. To our knowledge, the Fe isotopic composition of serpentine has never been measured prior to this study and we posit that the light isotopic compositions observed are a function of weak bond strength in the crystal lattice of the serpentine veins relative to the bond strength in olivine, awaruite, or magnetite.

The presence of the magnetite-awaruite pair with the predicted sense of fractionation with respect to the Mössbauer model allows for the calculation of equilibration temperature for this mineral pair formation (Fig. 8a). The isotopic fractionation factor between magnetite and awaruite intersects the Mössbauer model from Polyakov et al. (2007) at 335 + 82/−59 °C; uncertainty propagated from uncertainty of isotopic compositions. The mineralogy of New Caledonia serpentine veins is dominated by lizardite serpentine, which generally indicates formation temperatures less than ~300 °C (Evans, 2004), however lizardite stability can extend to much higher temperatures depending on composition (e.g., Caruso and Chernosky, 1979). The transition between the serpentine polymorphs is sluggish and lizardite has been found to persist to the highest limits of serpentine stability (Mellini et al., 1987). While this sluggish transformation occurs during prograde metamorphism, it nonetheless implies that the temperature at which lizardite can exist is poorly constrained. Thus our calculated temperature for co-existing magnetite and awaruite either extends the upper end of the thermodynamic stability field for lizardite or suggests that lizardite is metastable at these temperatures. Importantly, the temperature obtained from the magnetite-awaruite pair is substantially higher than fluids being emitted from springs in New Caledonia, which range from ~23 to 40 °C. Further, this result suggests that the serpentinization recorded in NC09-5 occurred in a much higher temperature environment, either within a subduction zone or in an oceanic seafloor hydrothermal system.

Awaruite (native Fe-Ni alloy) has no ionic bonds, therefore the ionic fractionation model recently proposed for inter-mineral fractionation in mantle xenoliths (Macris et al., 2015) is not directly applicable to awaruite. However, the ionic fractionation model does predict that "heavy Fe"

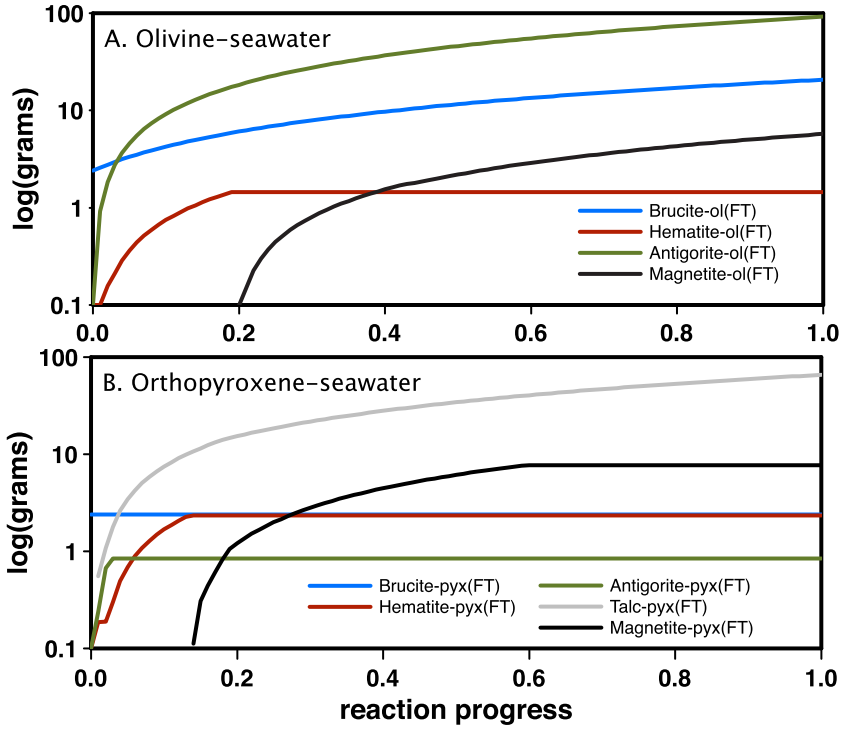

Fig. 5. Mineral assemblages precipitated during flow through model reactions between seawater and olivine (a) and pyroxene (b). Minor amounts (<0.1 g) of anhydrite and pyrite are not shown. Mineral assemblages for flow through models are identical to those from equilibrium titration models. In contrast to equilibrium titration models, the first minerals precipitated during the reactions remain for the entire reaction (e.g., hematite remains throughout the reaction, rather than being totally replaced by magnetite).

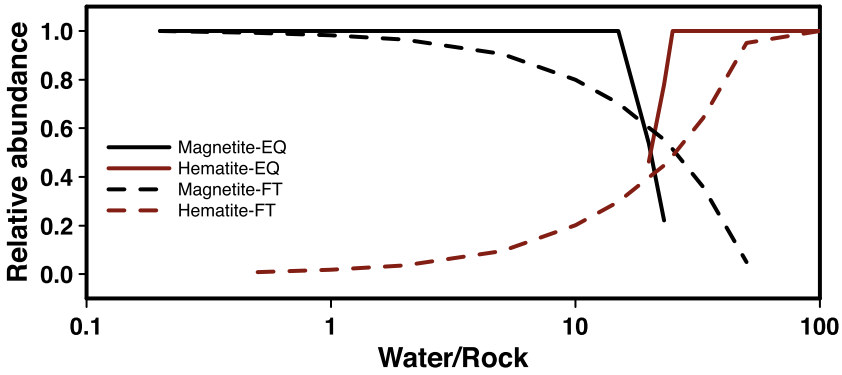

Fig. 6. Diagram illustrating the final oxide assemblages of equilibrium titration and flow through model reactions between olivine and seawater. The *y*-axis shows the relative abundances of hematite and magnetite compared to the total oxides (magnetite + hematite), while the *x*-axis shows the water:rock ratio. As the water:rock ratio decreases, the relative abundance of hematite decreases. The transition between hematite dominated to magnetite dominated oxides occurs over a smaller range of water:rock ratios in equilibrium titration models.

(high δ^{56}Fe and δ^{57}Fe) tends to fractionate into minerals with stronger bond strengths, consistent with the observed high δ^{56}Fe and δ^{57}Fe in magnetite. On the other hand, the "light Fe" in serpentine and all other phases (olivine, orthopyroxene) relative to magnetite indicates that Fe is weakly bonded in the serpentine structure.

The Fe isotopic compositions of the olivine and pyroxene (protolith assemblage) can also be used to place constrains on equilibration temperatures of the protolith rock. Both the Mössbauer model (Polyakov, 1997; Polyakov and Mineev, 2000; Polyakov et al., 2007) and the ionic model (Macris et al., 2015) predict measurable fractionations between olivine and orthopyroxene (greater than 1‰ difference in δ^{57}Fe in the ionic model) at the temperatures recorded by the magnetite and awaruite (~335 °C). The nearly identical Fe isotope composition between olivine and pyroxene suggests that these minerals equilibrated at much higher temperatures than the serpentine assemblage, regardless of the fractionation model used. Using the average compositions of olivine

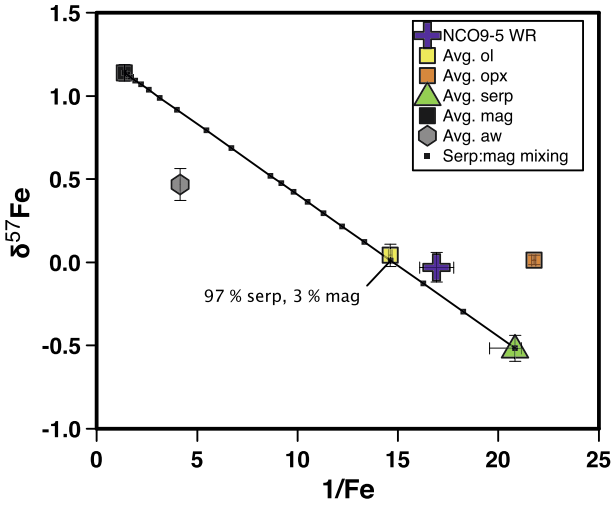

Fig. 7. Diagram of the mass balance relationships between minerals in NC09-5 using average values for Fe concentration and isotopic composition. Mixing models between 3% magnetite and 97% serpentine + brucite reproduce the observed composition of olivine. The whole rock has slightly lower Fe concentration due to presence of orthopyroxene.

and orthopyroxene from NC09-5, the Mössbauer model predicts temperatures consistent with equilibration in the mantle (Fig. 8b). Using the more Mg-rich enstatite composition, we obtain a temperature of $1325 + \infty/-708$ °C. This model produces the minimum possible temperature for any olivine-enstatite calculation (shown in Fig. 8b), and while the error is large, this temperature is not within error of the calculated temperature for magnetite-awaruite (Fig. 8b). This measurable difference demonstrates that the isotopic variations between the protolith assemblage and serpentine assemblage record two distinct equilibration temperatures and/or distinct periods of time.

5.3. Fe mobility and isotopic fractionation during hydrothermal processes

High temperature fluids emanating from ultramafic-hosted vents (Douville et al., 2002; Severmann et al., 2004), experimental work (Seyfried and Dibble, 1980; Janecky and Seyfried, 1986; Seyfried et al., 2007), and geochemical modeling results described in Section 4.3 all indicate that Fe concentrations increase in the fluid as serpentinization reactions proceed (Fig. 9). The uniformity in Fe isotopic composition of olivine, orthopyroxene and the bulk rock suggests that either: (1) no Fe was lost from the bulk rock; (2) any Fe lost from the bulk rock had the same isotopic composition as the bulk rock (i.e., $\delta^{56}Fe \sim 0.00‰$); or, (3) the amount of Fe lost from the bulk rock is insignificant relative to its total Fe content. However, Fe contents of fluids suggest the potential for large scale Fe mobility exists. Large fractionations between mineral phases and geochemical data can provide constraints on mass balance relationships affecting Fe.

In the reactions (Eqs. (1) and (2) in Section 2) taking place during serpentinization in New Caledonia (Frost et al., 2013) several chemical changes occur: (1) the amount of brucite decreases relative to serpentine in the veins; (2) native FeNi alloys are precipitated; and, (3) as the reaction proceeds free hydrogen forms and additional fluid evolves such that a pore fluid is maintained throughout the serpentinization process. The formation of magnetite (and fluid) occurs during the second reaction in Section 2 and this process produces fluid components during the formation of magnetite from brucite. Fe concentrations in the fluids from both experiments and geochemical modeling range from ~0.1 to 20 mmol/kg in the presence of brucite, magnetite, and serpentine, broadly consistent with observed concentrations of seafloor hydrothermal fluids (Fig. 9). These data suggest that as the fluid producing reaction proceeds, the Fe concentration increases in the fluid. In addition, it is likely that the fluid evolves toward a state of equilibrium, but never reaches equilibrium, with the rock during the serpentinization process.

Based on the predicted chemical reactions and mass balance constraints, the amount of water (and Fe) potentially removed from the system can be estimated. Mass balance between magnetite and serpentine indicate ~3% magnetite and ~97% serpentine (+ brucite) is required for vein compositions to be equivalent to the bulk rock composition of $\delta^{56}Fe \sim 0.00‰$ (discussed in Section 5.1). Frost et al. (2013) calculate that the particular phase proportions in NC09-5 represent ~30% serpentinization. In addition, the relative proportions of type 2 vs. type 1 veins (i.e., magnetite free) suggest that the type 2 veins are at most half of the serpentinized portion of the rock. If ~15% of the rock (NC09-5) contains type 2 veins, which are 3% magnetite by weight, then the total rock contains roughly ~0.45 weight percent magnetite. Reaction (2), above, indicates that 4 mol of H_2O are created for every 3 mol of magnetite created from 15 mol of brucite. Using the estimate of 4.5 g (0.0194 mol) of magnetite/kg of rock, only 0.44 g (0.0259 mol) of H_2O formed per kg of rock in the serpentinizing environment preserved in NC09-05. Using the highest estimate for the Fe concentrations of the pore fluid estimated from experimental data and geochemical modeling (~20 mmol/kg), as much as 0.0005 g of Fe per kg of rock could be present in the pore fluid generated by the formation of magnetite. There is 5.91 wt.% Fe in the rock (i.e., 1.06 mol Fe/kg rock). Thus, the 0.0005 g ($\sim 9 \times 10^{-6}$ moles) of Fe removed in the pore fluid is insignificant relative to the total Fe in the bulk rock, and movement of this pore fluid would not appreciably affect the bulk rock Fe concentration or isotopic composition regardless of the isotopic composition of the fluid. In fact, the maximum amount of fluid moving through and extracting Fe from the system can be estimated to place a maximum constraint on the water-rock ratio. Fig. 10 shows the whole rock $\delta^{57}Fe$ composition as function of LOI (loss on ignition) for abyssal serpentinites (Craddock et al., 2013), ophiolite serpentinites (Su et al., 2015; Debret et al., 2016), and NC09-5, overlain by a curve showing the effects of the water/rock ratio on bulk rock composition. The water/rock ratio must exceed 10:1 to appreciably effect the bulk rock Fe isotopic composition outside of the error of our measurements. Previous studies have estimate

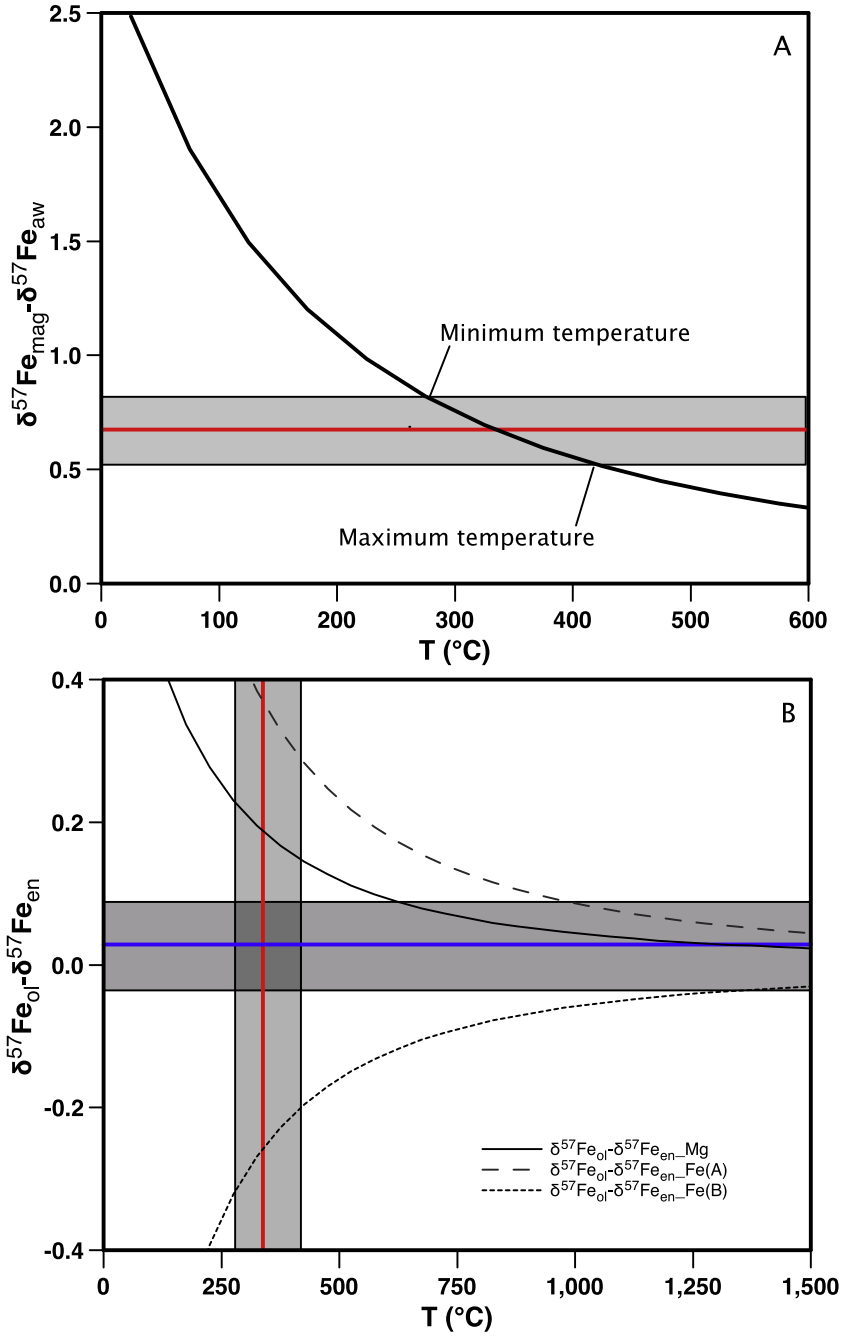

Fig. 8. (A) Isotopic fractionation factor between magnetite and awaruite (native Fe metal) as a function of temperature (black curve) based on Mossbauer spectroscopy and nuclear elastic resonant X-ray scattering (INRXS) models of Polyakov et al., 2007. The red line indicates the measured fractionation factor between magnetite and awaruite, with the gray field representing the possible range of fractionation factors accounting for measurement errors. The curve ($\delta^{57}Fe_{mag} - \delta^{57}Fe_{aw}$) is calculated using $\ln(\beta)_{mag} - \ln(\beta)_{aw}$, where $10^3\ln(\beta) = A_1{}^* (10^6/T^2) + A_2{}^* (10^6/T^2)^2 + A_3{}^* (10^6/T^2)^3$, A_1, A_2, and A_3 are coefficients, and T is temperature, in Kelvin. For magnetite, $A_1 = 0.95706$, $A_2 = -4.7296 \times 10^{-3}$, and $A_3 = 4.0703 \times 10^{-6}$. For awaruite (iron metal), $A_1 = 0.69964$, $A_2 = -1.4762 \times 10^{-3}$, and $A_3 = 4.8454 \times 10^{-6}$. (B) Isotopic fractionation factor between olivine and enstatite as a function of temperature for three Mossbauer spectroscopy models (Polyakov and Mineev, 2000). The three enstatite curves show a Mg-rich composition, and the A and B crystal substitution sites in a more Fe-rich enstatite composition. The blue line and gray field represent the measured fractionation factor between enstatite and olivine, and the red line represents the temperature calculated from the magnetite-awaruite curve in A. The gray fields represent the possible range of fractionation factors accounting for measurement errors. The minimum temperature calculated for olivine-enstatite (617 °C) is not within error of the maximum temperature calculated for the magnetite awaruite (417 °C). The fractionation curves in (A) and (B) use the same fractionation factor calculations. (For interpretation of the references to color in this figure legend, the reader is referred to the web version of this article.)

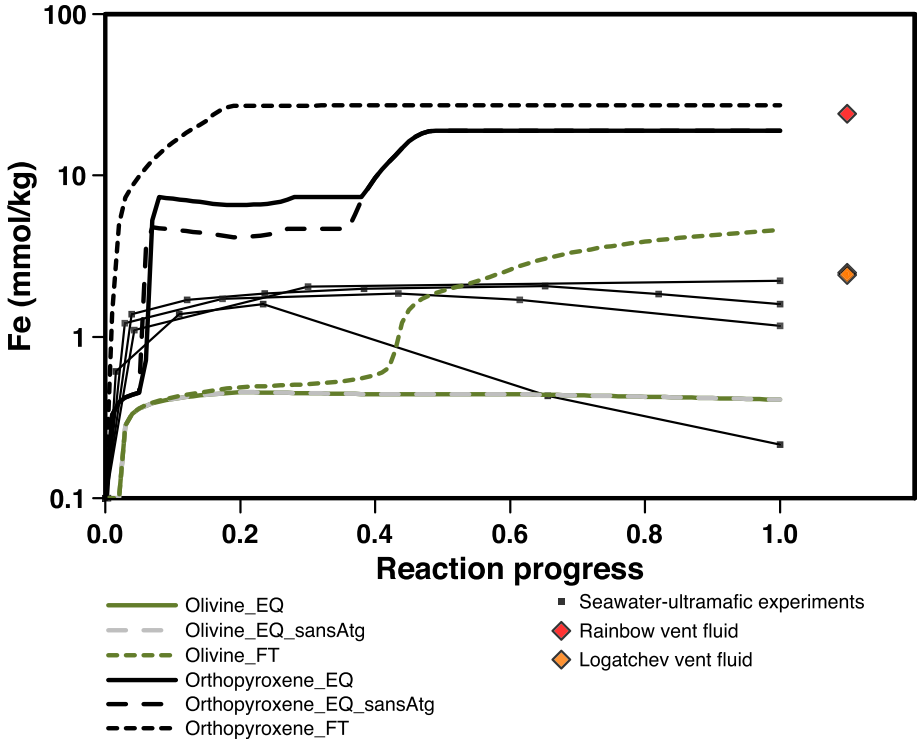

Fig. 9. Diagram comparing the Fe concentration from GWB models (thick lines), experimental data (thin black lines; Seyfried and Dibble, 1980; Janecky and Seyfried, 1986), and ultramafic-hosted vent fluids (Charlou et al., 2002; Schmidt et al., 2007). Experimental reactions are normalized to reaction progress (from 0 to 1) for comparison to geochemical models. Final fluid Fe concentrations range from ~0.1 to >20 mmol/kg. Geochemical modeling, experiments, and vent fluid compositions suggest that Fe is present in solution during the serpentinization process.

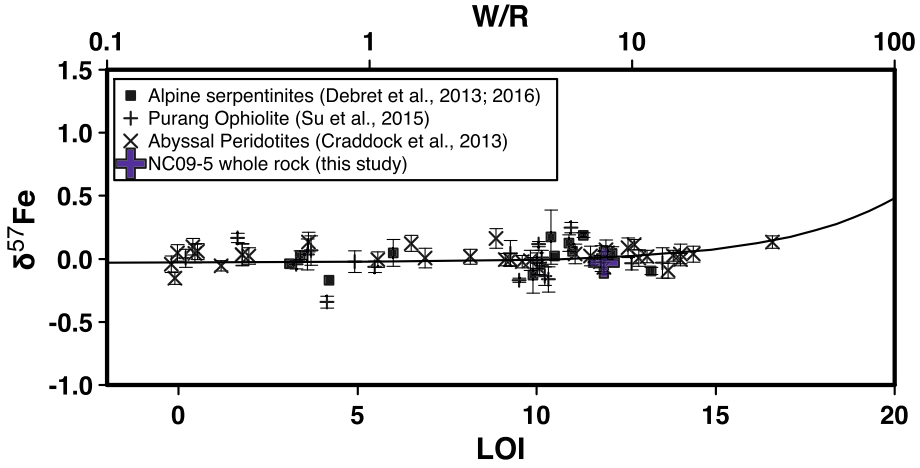

Fig. 10. Diagram showing the Fe isotopic composition of abyssal serpentinites and ophiolites as a function of LOI (loss on ignition), which is interpreted to reflect the degree of serpentinization (higher LOI = higher degree of serpentinization). The curve shows the effects of water:rock ratio on the bulk rock Fe isotopic composition, assuming a relatively high Fe concentration of ~20 mmol/kg and $\delta^{57}Fe = -0.30‰$. The curve shows that the bulk rock Fe isotopic composition is not significantly affected by fluid-rock interaction until water:rock ratios >~10.

water/rock ratios both above and below this estimate based on other isotope systematics (e.g., Sr and O isotopes in the upper crustal section of the Samail ophiolite, McCulloch et al., 1981).

This model proposes a pore fluid component formed by consumption of brucite to form magnetite, and this fluid likely leaves the serpentinizing system prior to tectonic un-roofing and exposure of the rock at the surface. Depending on the geologic setting of the final equilibration period of serpentinization, the fluid could either be expelled into ocean water during seafloor venting or alternatively forced into overlying continental lithosphere or the mantle wedge

during subduction. To address the first possibility of seafloor venting, Fig. 11 shows our mineral separate data compared to the Fe isotopic compositions and weight fractions of hydrothermal vent fluids (Sharma et al., 2001; Beard et al., 2003; Severmann et al., 2004; Rouxel et al., 2008) and seafloor vent sulfides (Rouxel et al., 2008). Based on the isotopic compositions and Fe concentrations of these hydrothermal features, we propose that fluids with higher Fe concentrations and higher Fe isotopic compositions have experienced more water-rock interaction. Whereas the pore fluid components we predict might attain a state of equilibrium with the rock, once the fluid exits the serpentinizing system in an oceanic hydrothermal system, it likely ascends rapidly. In contrast, serpentinizing pore fluids in a subduction zone setting would migrate into overlying rocks producing additional fluid alteration. While at some depth this type of fluid flux process likely leads to partial melting and arc-volcanism, the relatively low temperatures recorded in NC09-5 suggest this system did not reach depths associated with mantle melting. Thus, fluids leaving the serpentinizing system in NC09-5 would only produce relatively low temperature fluid alteration in overlying rocks. Once the fluid leaves the serpentinizing system, whether in an oceanic or subduction zone setting, open system processes may occur as discussed below. The New Caledonia ophiolite represents a hydrated mantle wedge, but hydration of olivine and the associated Fe isotopic fractionations likely occur in any geologic setting where serpentinization occurs.

In an oceanic hydrothermal vent, precipitation of sulfides likely occurs during ascent and venting, which would decrease the Fe content of fluids and potentially alter the isotopic composition of the fluid as well. Precipitation of sulfides would also require dissolved sulfur in the serpentinizing fluid. Because of the highly reducing nature of serpentinites, sulfur tends to be driven into the fluid phase during the early stages of serpentinization, where it resides as H_2S (Frost, 1985). In the most extreme conditions, serpentinites can inherit high amounts of sulfur due to significant addition of hydrothermal mineral precipitates (Alt et al., 2013). In addition, as the reducing capacity of peridotites is exhausted sulfide is no longer stable in solution (Klein and Bach, 2009). Abundant magnetite, virtually no sulfide observed in SEM images and abundant relict olivine in NC09-5 (Frost et al., 2013) suggests that the system could still evolve to higher degrees of serpentinization, maintaining a high reducing capacity in the fluid and preventing sulfide precipitation. Movement of sulfur is recorded in ODP Hole 1068, which is interpreted to have penetrated a fossil hydrothermal vent in serpentinite (Beard and Hopkinson, 2000). Carbonate veins containing marcasite and rare pyrrhotite occur in the breccia above the serpentinite. These veins and are thought to have been precipitated by fluids draining out of the serpentinite. The Fe isotopic compositions of marcasite from seafloor hydrothermal deposits are typically within the range defined by pyrite and chalcopyrite (Rouxel et al., 2003, 2008). Despite the fact that these sulfides were precipitated in mafic hydrothermal system, they provide our best estimate for sulfide compositions that may exist in ultramafic settings. Consequently, we posit that if any open system sulfide precipitation were to occur, the pore fluid would evolve to heavier isotopic compositions and lower Fe concentrations.

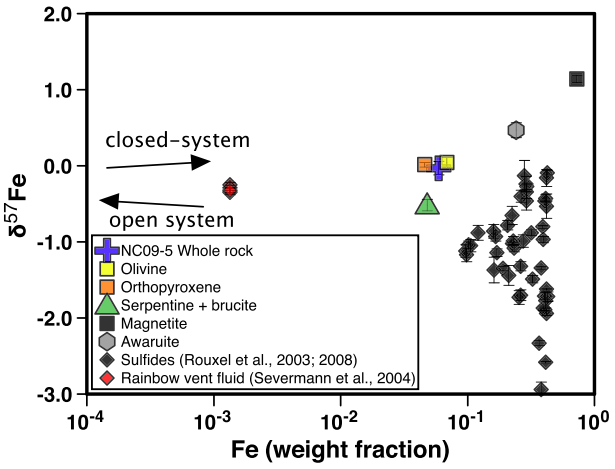

Fig. 11. δ^{57}Fe as a function of Fe weight fraction for New Caledonia mineral separates, ultramafic hosted seafloor hydrothermal vent fluids, and seafloor sulfides. The pore fluid present in the serpentinizing environment likely evolves to higher Fe concentrations as the reactions proceed until it is forced from the serpentinizing environment. Once the pore fluid is evacuated, open system processes (dilution or sulfide precipitation) would cause a decrease in the Fe concentrations of the fluid. The Fe weight fraction of seawater is $\sim 5 \times 10^{-8}$ and plots to the left of the x-axis on this diagram. Sulfide data from Rouxel et al. (2003, 2008) are from mafic hydrothermal systems, but nevertheless provide the best estimate for sulfide compositions that may precipitate in an open system environment.

Another possibility for open system processes affecting the pore fluid prior to venting in a seafloor hydrothermal setting is seawater dilution. While some seawater dilution is likely, the amount of seawater required to significantly change the concentration of Fe is greater than the extent of seawater dilution inferred from other parameters (Rouxel et al., 2008). For example, hydrothermal fluids are typically emitted from the seafloor at high temperatures relative to the surrounding seawater, in some cases approaching temperatures of 400 °C (Von Damm et al., 1997; Von Damm, 2000; Rouxel et al., 2008). Our mineral separate data indicate that the serpentinization process occurred at relatively high temperatures in NC09-05 (~335 °C, shown in Fig. 8a), consistent with temperatures found in many hydrothermal vent systems. In addition, most major element concentrations of vent fluids are not consistent with significant dilution by seawater (e.g., Mg, Rouxel et al., 2008). However, this does not necessarily rule out the possibility for seawater dilution entirely, as seawater must also be percolating into the crust simultaneously to supply the deep hydrothermal system with additional fluid.

Despite the relatively minor amount of Fe removed from the system compared to the total amount of Fe in the bulk rock, our data suggests that Fe is mobilized during hydration of ultramafic oceanic lithosphere on at least the grain scale. Recent work on serpentinites thought to represent the down going slab in a subduction zone has posited that Fe is mobile on larger scales during dehydration

reactions in the hotter/deeper parts of subduction zones (Debret et al., 2016). Fe isotopic compositions of whole rock serpentinites ranging from relatively shallow, low-temperature to deep, high-temperature settings become "heavier" (i.e. higher $\delta^{56}Fe$) as the degree of metamorphism increases. This isotopic trend is interpreted to reflect preferential removal of Fe^{2+} in serpentinite-derived fluids during subduction. The bulk-rock chosen for our study, a lizardite-dominated partially serpentinized dunite, has an Fe isotopic composition consistent with those reported for abyssal serpentinites (Craddock et al., 2013) and alpine lizardite serpentinites by Debret et al. (2016). In addition, the temperatures calculated for our serpentinite assemblage and prior knowledge of the tectonic history of New Caledonia indicate that this rock would have been serpentinized in the shallow parts of the mantle wedge, where large scale mobility of Fe is not likely to occur.

Regardless of the geologic setting of serpentinization, the sample's petrology and measured Fe isotope fractionations suggest the following timeline for fluid evolution during serpentinization:

Stage 1: Initial fluid infiltration and reaction: olivine + H_2O → serpentine + brucite. This reaction leads to the initial "mesh-texture" observed in many partially serpentinized rocks (e.g., Wicks and Whittaker, 1977; Bach et al., 2006; Katayama et al., 2010; Miyoshi et al., 2014). In addition, this reaction proceeds as isochemical hydration (i.e., only water is added, and nothing is removed; Bach et al., 2006). Note we do not have any direct measurements of this processes, as it is difficult to definitively separate type 1 veins for isotopic analysis. In addition, because the olivine grains are all within error of $\delta^{56}Fe = 0.00‰$, we suggest that Fe isotope fractionation was probably minimal during type 1 vein formation. It is likely that some of these veins existed in the olivine mineral separates we analyzed, however more detailed spatial analyses are required for analysis of type 1 veins.

Stage 2: Further fluid infiltration and transition from brucite to magnetite: brucite + SiO_2(aq) → serpentine + magnetite + H_2O + H_2. This overall reaction (see Eq. (2) in Section 2), represents the transition from the initial hydration stage to magnetite formation. The large Fe isotope fractionations measured in our study occur during this stage. Whereas an external source of SiO_2 is required, during this reaction serpentine (low $\delta^{56}Fe$) + magnetite (highest $\delta^{56}Fe$) + awaruite (high $\delta^{56}Fe$) + H_2O + H_2 may be in equilibrium. At this time the fluid evolves toward a state of equilibrium with the rock and becomes progressively enriched in Fe as the reaction proceeds. This reaction continues until the geologic environment forces the fluid from the pore space in the serpentinizing environment and the rock experiences no further mineralogical evolution (Fig. 12). In addition, armouring of the intact interior olivine grains may prevent further reaction prior to fluid release.

Stage 3: Escape of pore fluid into overlying environment: Pore fluid initially evolving in equilibrium with the type-2 vein assemblage is forced from the

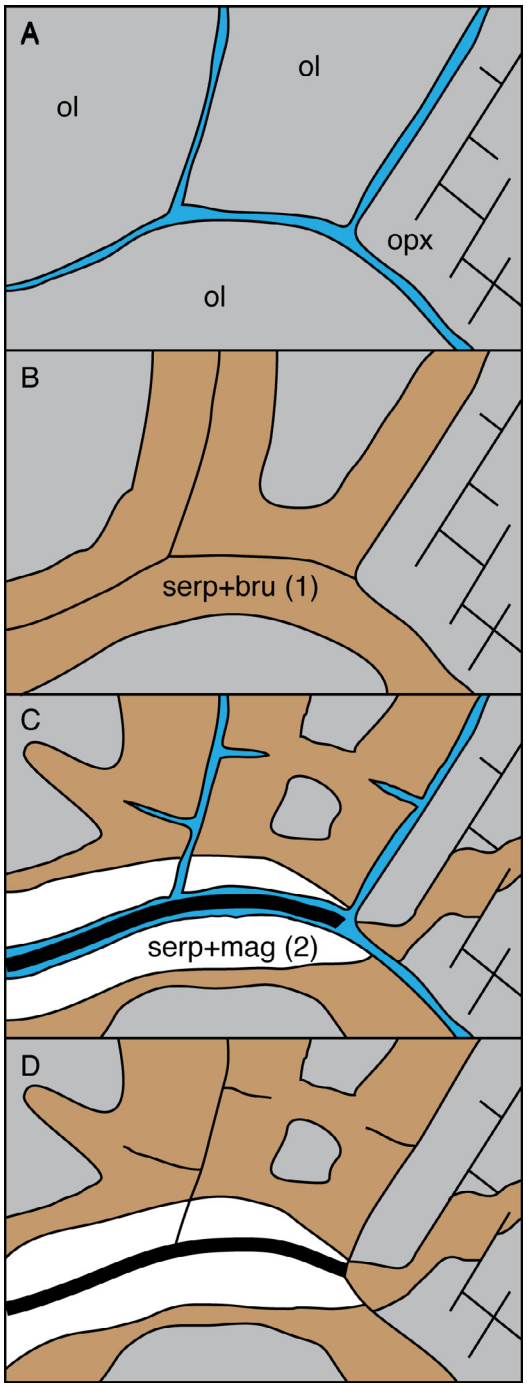

Fig. 12. Illustration of mineralogical evolution during serpentinization of NC09-05 from New Caledonia. (A) Initial fluid infiltration. (B) Absorption of fluid into the olivine protolith mineral to form serpentine and brucite (type 1 veins described by Frost et al., 2013). The reactions taking place from A to B are described by Eq. (1). (C) Reaction of brucite in type 1 veins with aqueous silica derived from pyroxene hydration to form serpentine, magnetite, awaruite, water, and hydrogen. A free fluid phase must persist during this time (i.e., it is not entirely absorbed by olivine to form type 1 veins). The reactions taking place from B to C are described by Eq. (2). (D) Final conditions post alteration (i.e., the current sample condition). Note no mineralogical changes occur from C to D and the fluid present in C is removed from the system.

serpentinizing environment. Depending on the geologic setting, this fluid is either venting into the ocean through a seafloor hydrothermal system, or forced into overlying crust in a subduction zone. In a seafloor vent system, this fluid could evolve by either precipitation of hydrothermal minerals and/or seawater dilution. In a subduction zone, this fluid produces hydrothermal alteration in the overlying rocks, either in the mantle wedge or shallow continental lithosphere.

6. CONCLUSIONS

In this study we measured Fe isotopic compositions in mineral separates from a partially-serpentinized dunite from New Caledonia to investigate the early stages of serpentinization. Our results show that magnetite and awaruite have high δ^{56}Fe and δ^{57}Fe values relative to olivine, while serpentine has relatively low δ^{56}Fe and δ^{57}Fe relative to olivine, broadly consistent with predicted equilibrium fractionation factors based upon the Mössbauer model (Polyakov, 1997; Polyakov and Mineev, 2000; Polyakov et al., 2007). These observed fractionations provide important insight into the scale of Fe mobility during the early stages of serpentinization, specifically:

(1) Initial hydration, brucite consumption and magnetite formation, followed by fluid escape, occurs regardless of the geologic setting (either in oceanic settings or subduction zones). Once released, this fluid will evolve differently depending on the geologic setting.
(2) The observed large Fe isotope fractionation between mineral phases occurs during formation of magnetite +/− native Fe. Fractionation between these mineral pairs indicates a formation temperature of 335 + 82/−59 °C based on the Mossbauer spectroscopy model of Polyakov et al. (2007). Calculations using olivine-orthopyroxene yield temperatures higher than, and not within error of, the magnetite-awaruite temperature for the serpentine assemblage. These results show that Fe isotopes in NC09-5 reflect two distinct periods of time and/or temperatures of equilibration. In addition, the use of Fe isotopes to evaluate temperature regimes in serpentinites shows potential for future studies of serpentinite mineral separates.
(3) The reactions taking place during serpentinization require the presence of a fluid phase. This fluid phase becomes progressively enriched in Fe as it resides in the pore space during serpentinization. Fe distribution between the fluid and resulting serpentine mineral assemblage records evolution toward equilibrium.
(4) Pore fluid forced from the serpentinizing environment is either vented into the ocean or migrates into overlying rocks in a subduction zone. Hydrothermal mineral precipitation and seawater dilution may occur as open system processes, and could decrease the Fe concentration of the fluid. In oceanic settings, this fluid migrates out of the system and feeds seafloor hydrothermal vents. In subduction zones, the fluid would likely migrate into overlying rocks, however, temperature recorded in NC09-5 suggest this fluid flux would be too shallow for partial melting in the mantle.

ACKNOWLEDGEMENTS

This work was supported by the National Science Foundation grants EAR 0960270 and OCE 1634669 awarded to KWWS. Three anonymous reviews and the editorial handling of Stephan Weyer substantially improved the quality and scope of this manuscript. We thank Bernhard Puecker-Ehrenbrink for using the WHOI EPD to disaggregate the sample for mineral separation, and Jim Beard, Wolfgang Bach, and Esther Schwarzenbach for thoughtful discussion on serpentinization. We thank John Kaszuba for insights into Geochemist's Workbench modeling.

REFERENCES

Aitchison J. C., Clarke G. L., Meffre S. and Cluzel D. (1995) Eocene arc-continent collision in New Caledonia and implications for regional southwest Pacific tectonic evolution. *Geology* **23**, 161–164.

Allen D. E. and Seyfried, Jr., W. E. (2004) Compositional controls on vent fluids from ultramafic-hosted hydrothermal systems ad mid-ocean ridges: An experimental study at 400 °C, 500 bars. *Geochim. Cosmochim. Acta* **67**, 1531–1542.

Alt J. C., Schwarzenbach E. M., Früh-Green G. L., Shanks, III, W. C., Bernasconi S. M., Garrido C. J., Crispini L., Gaggero L., Padrón-Navarta J. A. and Marchesi C. (2013) The role of serpentinities in cycling of carbon and sulfur: Seafloor serpentinization and subduction metamorphism. *Lithos* **178**, 40–54.

Andreani M., Muñoz M., Marcaillou C. and Delacour A. (2013) MXANES study of iron redox state in serpentine during oceanic serpentinization. *Lithos* **178**, 70–83.

Bach W., Paulick H., Garrido C. J., Ildefonse B., Meurer W. P. and Humphris S. E. (2006) Unraveling the sequence of serpentinization reactions: petrography, mineral chemistry, and petrophysics of serpentinites from MAR 15 °N (ODP Let 209, Site 1274). *Geophys. Res. Lett.* **33**. http://dx.doi.org/10.1029/2006GL025681.

Barnes I., O'Neil J. R. and Trescases J. J. (1978) Present day serpentinization in New Caledonia, Oman and Yugoslavia. *Geochim. Cosmochim. Acta* **42**, 144–145.

Barnes J. D., Eldam R., Lee C. A., Errico J. C., Loewy S. and Cisneros M. (2013) Petrogenesis of serpentinites from the Franciscan Complex, western California, USA. *Lithos* **178**, 143–157.

Beard J. S. and Hopkinson L. (2000) A fossil, serpentinization-related hydrothermal vent, Ocean Drilling Program Leg 173, Site 1068 (Iberia Abyssal Plain): Some aspects of mineral and fluid chemistry. *J. Geophys. Res.* **105**, 16527–16539.

Beard B. L., Johnson C. M., Skulan J. L., Nealson K. H., Cox L. and Sun H. (2003) Application of Fe isotopes to tracing the geochemical and biological cycling of Fe. *Chem. Geol.* **195**, 87–117.

Beard J. S., Frost B. R., Fryer P., McCaig A., Searly R., Ildefonse B., Zinin P. and Sharma S. K. (2009) Onset and progression of serpentinization and magnetite formation in olivine-rich troctolite from IODP Hole U1309D. *J. Pet.* **50**, 387–403.

Bethke, C., Yeakel, S. (2012). *The Geochemist Workbench release 9.0*. Champaign, Illinois.

Boudier F., Baronnet A. and Mainprice D. (2010) Serpentine mineral replacement of natural olivine and their seismic implications: Oceanic lizardite versus subduction-related antigorite. *J. Pet.* **51**, 495–512.

Bromiley G. D. and Pawley A. R. (2003) The stability of antigorite in the systems MgO-SiO2-H2O (MSH) and MgO-Al2O3-SiO2-H2O (MASH): The effects of Al3+ substitution on high-pressure stability. *Am. Min.* **88**, 99–108.

Brown, J., Colling, J., Park, D., Phillips, J., Rothery, D. Wright, J. (1989). Seawater: Its composition, properties and behavior. 165 p. Pergamon.

Cannat M., Mevel C., Maia M., Deplus C., Durand C., Gente P., Agrinier P., Belarouci A., Dubuisson G., Humler E. and Reynolds J. (1995) Thin crust, ultramafic exposures, and rugged faulting patterns at the Mid-Atlantic Ridge (22°-24 °N). *Geology* **23**, 49–52.

Carlson R. L. (2001) The abundance of ultramafic rocks in Atlantic Ocean crust. *Geophys. J. Int.* **144**, 37–48.

Caruso L. J. and Chernosky J. V. (1979) The stability of lizardite. *Can. Min.* **17**, 757–769.

Charlou J. L., Donval J. P., Fouquet Y., Jean-Baptiste P. and Holm N. (2002) Geochemistry of high H_2 and CH_4 vent fluids issuing from ultramafic rocks at Rainbow hydrothermal field (36 °14'N, MAR). *Chem. Geol.* **191**, 345–359.

Chavagnac V., Monnin C., Ceuleneer G., Boulart C. and Hoareau G. (2013) Characterization of hyperalkaline fluids produced by low-temperature serpentinization of mantle peridotites in the Oman and Ligurian ophiolites. *Geochem. Geophys. Geosys.* **14**, 2496–2522.

Cluzel D., Meffre S., Maurizot P. and Crawford A. J. (2006) Earliest Eocene (53 Ma) convergence in the Southwest Pacific: evidence from pre-obduction dikes in the ophiolite of New Caledonia. *Terra Nova* **18**, 395–402.

Coleman R. G. and Keith T. E. (1971) A chemical study of serpentinization – Burro Mountain, California. *J. Pet.* **12**, 311–328.

Craddock P. R. and Dauphas N. (2010) Iron isotopic compositions of geological reference materials and chondrites. *Geostand. Geoanal. Res.* **35**, 101–123.

Craddock P. R., Warren J. M. and Dauphas N. (2013) Abyssal peridotites reveal the near-chondritic Fe isotopic compositions of the Earth. *Earth Planet. Sci. Lett.* **365**, 63–76.

Debret B., Millet M.-A., Pons M.-L., Bouilhol P., Inglis E. and Williams H. (2016) Isotopic evidence for iron mobility during subduction. *Geology* **44**, 215–218.

Delaney J. R., Robigou V., McDuff R. E. and Tivey M. K. (1992) Geology of a vigorous hydrothermal system on the Endeavour Segment, Juan de Fuca Ridge. *J. Geophys. Res.* **97**, 19663–19682.

Deville E. and Prinzhofer A. (2016) The origin of N_2-H_2-CH_4-rich natural gas seepages in ophiolitic context: a major and noble gases study of fluid seepages in New Caledonia. *Chem. Geo.* **440**, 139–147.

Dideriksen K., Baker J. A. and Stipp S. L. S. (2006) Iron isotopes in natural carbonate minerals determined by MC-ICP-MS with a ^{58}Fe-^{54}Fe double spike. *Geochim. Cosmochim. Acta* **70**, 118–132.

Douville E., Charlou J. L., Oelkers E. H., Bienvenu P. and Jove Colon C., et al. (2002) The rainbow vent fluids (36 °14'N, MAR): the influence of ultramafic rocks and phase separation on trace metal content in Mid-Atlantic Ridge hydrothermal fluids. *Chem. Geo.* **184**, 37–48.

Evans B. W. (1977) Metamorphism of Alpine peridotite and serpentinite: *Ann. Rev. Earth Planet Sci.* **5**, 355–447.

Evans B. W. (2004) The serpentinite multisystem revisited: chrysotile is metastable. *Int. Geol. Rev.* **46**, 479–506.

Evans B. W. (2008) Control of the products of serpentinization by the $Fe^{2+}Mg_{-1}$ exchange potential of olivine and orthopyroxene. *J. Pet.* **49**, 1873–1887.

Evans B. W. (2010) Lizardite versus antigorite serpentinite: Magnetite, hydrogen, and life(?). *Geology* **38**, 879–882.

Evans K. A., Powell R. and Frost B. R. (2013) Using equilibrium thermodynamics in the study of metasomatic alteration, illustrated by an application to serpentinites. *Lithos* **168–169**, 67–84.

Frost B. R. (1985) On the stability of sulfides, oxides, and native metals in serpentinite. *J. Pet.* **26**, 31–63.

Frost B. R. and Beard J. S. (2007) On silica activity and serpentinization. *J. Pet.* **48**, 1351–1368.

Frost B. R., Beard J. S., McCaig A. and Condliffe E. (2008) The formation of micro-rodingites from IODP Hole 1309D: Key to understanding the process of serpentinization. *J. Pet.* **49**, 1579–1588.

Frost B. R., Evans K. A., Swapp S. M., Beward J. S. and Mothersole F. E. (2013) The process of serpentinization in dunite from New Caledonia. *Lithos* **178**, 24–39.

He Y., Ke S., Teng F., Wang T., Wu H., Lu Y. and Li S. (2015) High-precision iron isotope analysis of geological reference materials by high-resolution MC-ICP-MS. *Geostand. Geoanal. Res.* **39**, 341–356.

Hilairet N., Daniel I. and Reynard B. (2006) P-V equations of state and the relative stabilities of serpentine varieties. *Phys. Chem. Min.* **33**, 629–637.

Holland T. J. B. and Powell R. (2011) An improved and extended internally consistent thermodynamic dataset for phases of petrological interest, involving a new equation of state for solids. *J. Met. Pet.* **29**, 333–383.

Hyndman R. D. and Peacock S. M. (2003) Serpentinization of the forearc mantle. *Earth Planet. Sci. Lett.* **212**, 417–432.

Iyer K., Rüpke L. H. and Phipps Morgan J. (2010) Feedbacks between mantle hydration and hydrothermal convection at oceanic spreading centers. *Earth Planet. Sci. Lett.* **296**, 34–44.

Janecky D. R. and Seyfried W. E. (1986) Hydrothermal serpentinization of peridotite within the oceanic crust: Experimental investigations of mineralogy and major element chemistry. *Geochim. Cosmochim. Acta* **50**, 1357–1378.

Katayama I., Kurosaki I. and Hirauchi K. (2010) Low silica activity for hydrogen generation during serpentinization: An example of natural serpentinites in the Mineoka ophiolite complex, central Japan. *Earth Planet. Sci. Lett.* **298**, 199–204.

Kelley D. S., Karson J. A., Blackman D. K., Früh-Green G. L., Butterfield D. A., Lilley M. D., Olson E. J., Schrenk M. O., Roe K. K., Lebon G. T. and Rivizzigno P. (2001) An off-axis hydrothermal vent field near the Mid-Atlantic Ridge at 30 °N. *Nature* **412**, 145–149.

Klein F. and Bach W. (2009) Fe-Ni-Co-O-S phase relations in peridotites-seawater interactions. *J. Pet.* **50**, 37–59.

Klein F., Bach W., Humphris S. E., Kahl W., Jöns N., Moskowitz B. and Berquó T. S. (2014) Magnetite in seafloor serpentinite – Some like it hot. *Geology* **42**, 135–138.

Liu S., Li D., Li S., Teng F., Ke S., He Y. and Lu Y. (2014) High-precision copper and iron isotope analysis of igneous rock standards by MC-ICP-MS. *J. Anal. Atom. Spec.* **29**, 122–133.

Marques J. M., Carreira P. M., Rosário Carvalho M., Matias M. J., Goff F. E., Basto M. J., Graca R. C., Aires-Barros L. and Rocha L. (2008) Origins of high pH mineral waters from ultramafic rocks, Central Portugal. *Appl. Geochem.* **23**, 3278–3289.

Macris C. A., Manning C. E. and Young E. D. (2015) Crystal chemical constraints on inter-mineral Fe isotope fractionation and implications for Fe isotope disequilibrium in San Carlos mantle xenoliths. *Geochim. Cosmochim. Acta* **154**, 168–185.

McCollom T. M., Klein F., Robbins M., Moskowitz B., Berquó T. S., Jöns N., Bach W. and Templeton A. (2016) Temperature trends for reaction rates, hydrogen generation, and partitioning of iron during experimental serpentinization of olivine. *Geochim. Cosmochim. Acta* **181**, 175–200.

McCulloch M. T., Gregory R. T., Wasserburg G. J. and Taylor H. P. (1981) Sm-Nd, Rb-Sr, and 18O/16O systematics in an oceanic crustal section: Evidence from the Samail Ophiolite. *J. Geophys. Res.* **86**, 2721–2735.

Mellini M., Trommsdorff V. and Compagnoni R. (1987) Antigorite polysomatism: behaviour during progressive metamorphism. *Cont. Min. Pet.* **97**, 147–155.

Millet M., Baker J. and Payne C. (2012) Ultra-precise stable Fe isotope measurements by high resolution multiple-collector inductively coupled plasma mass spectrometry with a ^{57}Fe-^{58}Fe double spike. *Chem. Geo.* **304–305**, 18–25.

Miyoshi A., Kogiso T., Ishikawa N. and Mibe K. (2014) Role of silica for the progress of serpentinization reactions: Constraints from successive changes in mineralogical textures of serpentinites from Iwanaidake ultramafic body, Japan. *Am. Min.* **99**, 1035–1044.

Mothersole, F. E., Evans, K., Frost, B. R. (in press). A comparison of abyssal and hydrated mantle wedge serpentinised peridotites: implications for element transfer in subduction zones. Contrib. Min. Pet.

Polyakov V. B. (1997) Equilibrium fractionation of the iron isotopes: estimation from Mössbauer spectroscopy data. *Geochim. Cosmochim. Acta* **61**, 4213–4217.

Polyakov V. B. and Mineev S. D. (2000) The use of Mössbauer spectroscopy in stable isotope geochemistry. *Geochim. Cosmochim. Acta* **64**, 849–865.

Polyakov V. B., Clayton R. N., Horita J. and Mineev S. D. (2007) Equilibrium iron isotope fractionation factors of minerals: reevaluation from the data of nuclear inelastic resonant X-ray scattering and Mössbauer spectroscopy. *Geochim. Cosmochim. Acta* **71**, 3833–3846.

Rouméjon S. and Cannat M. (2014) Serpentinization of mantle-derived peridotites at mid-ocean ridges: Mesh texture development in the context of tectonic exhumation. *Geochem. Geophys. Geosys.* **15**, 2354–2379.

Rouxel O., Dobbek N., Ludden J. and Fouquet Y. (2003) Iron isotope fractionation during oceanic crust alteration. *Chem. Geol.* **202**, 155–182.

Rouxel O., Shanks, III, W. C., Bach W. and Edwards K. J. (2008) Integrated Fe- and S-isotope study of seafloor hydrothermal vents at East Pacific Rise 9–10 °N. *Chem. Geol.* **252**, 214–227.

Schmidt K., Koschinsky A., Garbe-Schönberg D., de Carvalho L. M. and Seifert R. (2007) Geochemistry of hydrothermal fluids from the ultramafic-hosted Logatchev hydrothermal field, 15 ° N on the Mid-Atlantic Ridge: Temporal and Spatial investigation. *Chem. Geo.* **242**, 1–21.

Severmann S., Johnson C. M., Beard B. L., German C. R., Edmonds H. N., Chiba H. and Green D. R. H. (2004) The effect of plume processes on the Fe isotope compositions of hydrothermally derived Fe in the deep ocean as inferred from the Rainbow vent site, Mid-Atlantic Ridge, 36 °14'N. *Earth Planet. Sci. Lett.* **225**, 63–76.

Seyfried W. E. and Dibble W. E. (1980) Seawater-peridotite interaction at 300 °C and 500 bars: implications for the origin of oceanic serpentinites. *Geochim. Cosmochim. Acta* **44**, 301–321.

Seyfried, Jr, W. E., Foustoukos DI. and Fu Qi. (2007) Redox evolution and mass transfer during serpentinization: an experimental and theoretical study at 200 degrees C, 500 bar with implications for ultramafic-hosted hydrothermal systems at mid-ocean ridges. *Geochem. Cosmochim. Acta* **71**, 3872–3886.

Seyfried, Jr, W. E., Pester NJ., Tutolo BM. and Ding. K. (2015) The Lost City hydrothermal system: Constraints imposed by vent fluid chemistry and reaction path models on subseafloor heat and mass transfer processes. *Geochim. Cosmochim. Acta* **163**, 59–79.

Sharma M., Polizzotto M. and Anbar A. D. (2001) Iron isotopes in hot springs along the Juan de Fuca Ridge. *Earth Planet. Sci. Lett.* **194**, 39–51.

Smith D. K., Cann J. R. and Escartín J. (2006) Widespread active detachment faulting and core complex formation near 13 °N on the Mid-Atlantic Ridge. *Nature* **442**, 440–443.

Streit E., Kelemen P. and Eiler, (2012) Coexisting serpentine and quartz from carbonate-bearing serpentinized peridodite in the Samail Ophiolite4, Oman. *Contrib. Min. Pet.* **164**, 821–837.

Su B., Teng F., Hu Y., Shi R., Zhou M., Zhu B., Liu F., Gong X., Huang Q., Xiao Y., Chen C. and He Y. (2015) Iron and magnesium isotope fractionation in oceanic lithosphere and sub-arc mantle: Perspectives from ophiolites. *Earth Planet. Sci. Lett.* **430**, 523–532.

Toft P. B., Arkanai-Hamed J. and Haggerty S. E. (1990) The effects of serpentinization on density and magnetic susceptibility: a petrophysical model. *Phys. Earth Planet Int.* **65**, 137–157.

Von Damm K. L., Butternmore L. G., Oosting S. E., Bray A. M., Fornari D. J., Lilley M. D. and Shanks, III, W. C. (1997) Direct observation of the evolution of a seafloor 'black smoker' from vapor to brine. *Earth Planet. Sci. Lett.* **149**, 101–111.

Von Damm K. L. (2000) Chemistry of hydrothermal vent fluids from 9°-10 °N, East Pacific Rise: ''Time zero'', the immediate posteruptive period. *J. Geophys. Res.* **105**, 11203–11222.

Weyer S. and Schwieters J. B. (2003) High precision Fe isotope measurements with high mass resolution MC-ICPMS. *Int. J. Mass. Spec.* **226**, 355–368.

Wicks F. J. and Whittaker E. J. W. (1977) Serpentine textures and serpentinization. *Can. Min.* **15**, 459–488.

Yogodzinski G. M., Brown S. T., Kelemen P. B., Vervoort J. D., Portnyagin M., Sims K. W. W., Hoernle K., Jicha B. R. and Werner R. (2015) The role of subducted basalt in the source of island arc magmas: Evidence from seafloor lavas of the Western Aluetians. *J. Pet.* **56**, 441–492.

Zhu X.-K., O'Nions R. K., Guo Y. and Reynolds B. C. (2000) Secular variation of iron isotopes in North Atlantic deep water. *Science* **287**, 2000–2002.

Associate editor: Stefan Weyer